Clays and Clay Minerals, Vol. 55, No. 2, 200–212, 2007.

SHORT-TERM HYDROTHERMAL EFFECTS ON THE 'CRYSTALLINITIES' OF ILLITE AND CHLORITE IN THE FOOTWALL OF THE AACHEN-FAILLE DU MIDI THRUST FAULT – FIRST RESULTS OF THE RWTH-1 DRILLING PROJECT

SVEN SINDERN[1,*], HELGE STANJEK[2], CHRISTOPH HILGERS[3] AND YVONNE ETOUNDI[4]

[1] Institute of Mineralogy and Economic Geology, RWTH Aachen University, Wüllnerstrasse 2, 52056 Aachen, Germany
[2] Clay and Interface Mineralogy, RWTH Aachen University, Wüllnerstrasse 2, 52056 Aachen, Germany
[3] Lehr und Forschungsgebiet Geologie und Endogene Dynamik, RWTH Aachen University, 52056 Aachen, Germany
[4] Ministère de l'Industrie, des Mines et du Développment Technologie – CAPM – BP. 15620, Yaoundé, Cameroun

Abstract—Investigation of material from three core sections of the RWTH-1 drill-hole in the Wurm syncline of Aachen, Germany, shows mineralogical and structural evidence of intensive hydrothermal activity in the footwall of the Aachen thrust. Mineral and microstructural data indicate minimum temperatures of 200–250ºC. $CIS_{illite\ 001}$ values of 0.45–0.61 ($\Delta^{o}2\theta$) and insignificant amounts of smectite indicate a late diagenetic grade for illite pointing to temperatures <200ºC. Chlorite, mainly formed in veins and cleavage planes, has $CIS_{chlorite\ 002}$ values between 0.35 and 0.26 ($\Delta^{o}2\theta$) which only in part point to anchizonal grade. In contrast to these illite and chlorite data, maximum temperatures up to 370ºC can be expected based on comparison with recently published fluid inclusion and mineral thermometric data. Illite is neither significantly affected by the hydrothermal event nor by deformation, and mirrors the burial history of the Wurm syncline.

Chlorite grew syntectonically as is shown by bent and predominantly stretched sheets which do not, however, have deformed structures. Syntectonic hydrothermal growth by incipient nucleation along crystal edges limited domain size and thus also the $CIS_{chlorite\ 002}$ values. The hydrothermal event did not last long enough to allow further crystal growth. The retarded CIS_{illite} and $CIS_{chlorite}$ grades can be best explained by limited duration (probably <5000 y) of the hydrothermal event which for a short time reached epithermal temperatures. The hydrothermal fluid flow was caused by dewatering of sedimentary rocks during thrusting and tectonic thickening within the Variscan orogen and it was focused along the Aachen thrust which represents the frontal Variscan thrust.

Key Words—Aachen, Chlorite, CIS, Crystallinity, Fluid Flow, Hydrothermal, Illite, Integral Breadth, Variscan Orogeny, Wurm Syncline.

INTRODUCTION

Clay minerals respond to increasing temperatures, pressures and changing fluid compositions by generating a reaction series, in which, *e.g.* smectites form mixed-layered phases, which, in turn increase in illite layers, until pure illite and finally muscovite is produced (Hower *et al*., 1976). This reaction series is accompanied by a progressive increase in crystal thicknesses ('illite crystallinity'), which shows up not only as increasingly sharper peaks in X-ray diffraction (XRD) patterns, but was verified by transmission electron microscopy (TEM) observations (*e.g.* Środoń *et al*., 1992; Árkai *et al*., 1996). This peak sharpening of illites was first used by Weaver (1960) and Kübler (1964) to determine and define diagenetic and very low-grade metamorphic zones. Being a complex, sometimes strictly empirical parameter, the full width at half maximum height (FWHM) of the 001 peak of illite served long as the Kübler index (KI), but it became increasingly obvious that KI is influenced by many parameters and must not be overinterpreted (Guggenheim *et al*., 2002; Jaboyedoff *et al*., 2001; Kübler and Jaboyedoff, 2000). For example, small amounts of swelling layers (*e.g.* Eberl and Velde, 1989) increase the peak breadth as do interstratifications with other non-illitic layers, *e.g.* paragonite or margarite (Battaglia *et al*., 2004). Apart from purely instrumental effects, which could be corrected by standards (Kisch, 1990; Warr, 1996), even the particle-size distribution itself influences the peak breadth (Langford *et al.*, 2000). Inclusion of other basal reflections in combination with fitting techniques (*e.g.* Lanson and Kübler, 1994) and/or simulations with Newmod (Eberl and Velde, 1989; Warr and Nieto, 1998) are therefore necessary to extract more information from the XRD patterns.

A quite different but related aspect of 'crystallinities' is the general question of whether we may interpret them in terms of thermodynamics or better in terms of kinetics. Merriman (2005) suggested that especially in low-*T* environments, sluggish reaction kinetics prevail over thermodynamic equilibrium (*e.g.* Robinson and Merriman, 1999; Essene and Peacor, 1995). Despite their attempt to minimize the free energy of the system, mineral assemblages and their properties reflect reaction

* E-mail address of corresponding author:
sindern@rwth-aachen.de
DOI: 10.1346/CCMN.2007.0550209

progress but not a thermodynamic equilibrium *sensu stricto*. As a consequence, it is not temperature itself which is mirrored in a mineral assemblage. Rather it is energy flux, which may comprise heat flow as well as tectonically induced strain energy – assuming that the chemical composition of a system stays relatively constant. In very high heat-flow geothermal systems, such as the Salton Sea geothermal field, clays reached the supermature stage during a heating event of only 10,000 y (Yau *et al*., 1988; Velde and Lanson, 1993). In a study of the East Slovak Basin, Clauer *et al*. (2003) distinguished between illite growth either controlled by burial or by hydrothermal activity.

Little is known, however, for a geological situation like a thrust system, in which strain energy as well as both burial and hydrothermal heat flow contributed to the total energy flux. Such a system is represented by the Variscan Aachen-Midi thrust in Germany, the northernmost large-scale thrust fault of the Variscan orogeny (Oncken *et al.*, 1999) with a displacement of at least 17 km (von Winterfeld, 1994). Increased vitrinite reflectance data within a few km to the N and S of the Aachen thrust point to enhanced heat flow up to 0.15 W/m^2 along this structure in Carboniferous times (Lünenschloss, 1998; Teichmüller and Teichmüller, 1979; von Winterfeld, 1994; Oncken *et al.*, 1999) which exceeds the present-day value for this region of 0.07–0.08 W/m^2 (Lünenschloss, 1998). Evidence of hydrothermal activity in this region is found in veins within core material of the 2544 m deep RWTH-1 geothermal well (Chatziliadou *et al.*, 2005; Lögering *et al.*, 2005, 2006) which was drilled in 2004 only 500 m to the north of the Aachen thrust. The aim of this work was therefore to test whether energy flux by strain, burial or short-termed hydrothermal heat flow have left interpretable fingerprints on illites and chlorites.

GEOLOGICAL SETTING

The site of the RWTH-1 drill-hole within the city of Aachen is located ~500 m to the north of the Aachen thrust which is the NE prolongation of the Faille de Midi (Oncken *et al.*, 1999). Along this south-dipping structure, Devonian to Carboniferous carbonaceous and siliciclastic units of the Aachen imbrication zone and the Venn-Weser-Inde nappe are thrust above the Wurm syncline (Figure 1). The upper 1000 m of the RWTH-1 drill-hole consists of Upper Carboniferous strata (Westfalian, Namurian, Österreich *et al.*, 2005). Marked by a characteristic change in lithofacies (Lundershausen *et al.*, 2005), these units are unconformably followed by Famennian shales and slates (in part equivalent to the Cheiloceras zone) up to 1448 m. The section from 1448 m to the end at 2544 m is predominantly composed of Lower Devonian sandstones and siltstones so far not described in detail. Cores were cut in the depth intervals 1392–1515 m, 2128–2143 m and 2536–2544 m. The first interval is characterized by intensive deformation and hydrothermal vein formation within a fault zone.

The compressive Variscan deformation and contemporaneous metamorphism in the Venn-Weser-Inde nappe was dated by Nierhoff (1994) at between 336 and 300 Ma on the basis of K-Ar analyses. Glasmacher *et al.* (2001) defined an age of 314±7 Ma for the Variscan cleavage deformation and a minimum age of 300±8 Ma for a late-stage hydrothermal fluid flow event using Ar-Ar dating. For the southern Venn-Weser-Inde nappe, peak temperatures of ~330ºC to 400ºC of the Variscan metamorphism are constrained by fluid-inclusion, mineral paragenesis, chlorite-thermometry and vitrinite data (Hilgers *et al.*, 2006; Vogtmann-Becker, 1990; Glasmacher, 1995; Oncken *et al.*, 1999; Zhang *et al.*, 1997) and Kübler index (epizonal grade, Tschernoster *et al.*, 1995). Based on vitrinite and fluid-inclusion data, Oncken *et al.* (1999) assumed that peak temperatures decrease to 250–280ºC in the northern part of the Venn-Weser-Inde nappe (Inde syncline).

In larger areas of the foreland of the Aachen thrust, lower temperatures can be expected. On the basis of mineralogical, textural and vitrinite reflectance data obtained in Carboniferous to Devonian rocks of the Liege syncline to the east of the Wurm syncline, Hollmann (1997) derived a temperature of 200ºC which is also consistent with maximum burial depths of 4.5 km (Rottke and Stroink, 1999). For the zone close to the Aachen thrust and especially for the Wurm syncline, detailed temperature information is mainly given by organic maturity data. Vitrinite reflectance, R_{max}, shows a correlation with stratigraphic position and ranges between 1.5 and 3.6% (Teichmüller and Teichmüller, 1979; von Winterfeld, 1994). For this region Fielitz and Mansy (1999) also reported temperatures of ~200ºC. Due to numerous vitrinite reflectance data within Carboniferous rocks (Babinecz, 1962; Teichmüller and Teichmüller, 1979; Steingrobe, 1990; von Winterfeld, 1994) it is well established that within the Upper Carboniferous of the Wurm syncline, vitrinite reflectance increases from north to south (Figure 1). One anomalously high R_{max} value of 6.70% in Famennian rocks in the city of Aachen was reported by von Winterfeld (1994), and Oncken *et al.* (1999) pointed to epizonal peak R_{max} values up to 7.3% at the Aachen-Midi thrust. Increased vitrinite reflectance is observed in the footwall of the Aachen-Midi thrust in a belt with a width of a few kilometres parallel to the Aachen-Midi thrust extending from the north of Aachen to Namur in Belgium (Knapp, 1980; von Winterfeld, 1994). Maturation of the organic material is older than deformation (Knapp, 1980) and therefore of Carboniferous age. The increased values of vitrinite reflectance along the Aachen thrust are explained by enhanced heat flow close to this structure during upper Carboniferous times (Teichmüller and Teichmüller, 1979; Knapp, 1980).

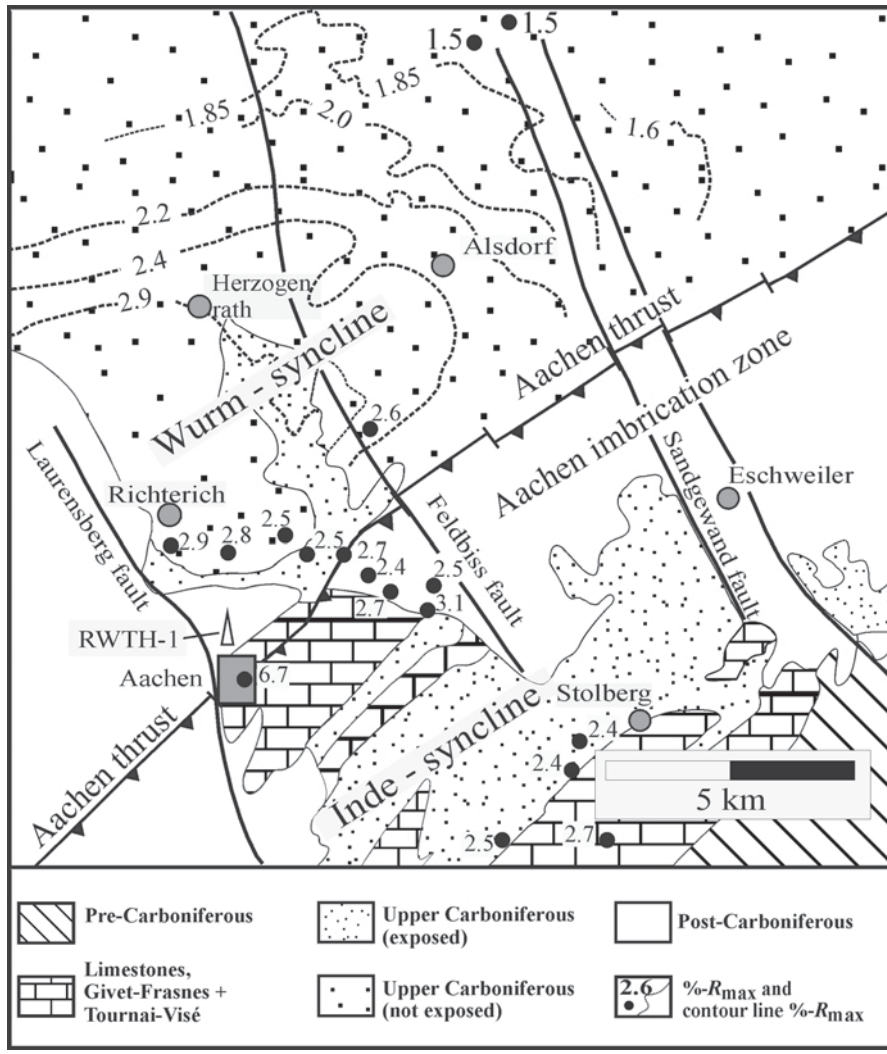

Figure 1. Geological sketch map of the RWTH-1 drill-hole location and the Aachen region, modified from Steingrobe (1990). Figures indicate the vitrinite reflectance (%-R_{max}) within Upper Carboniferous sediments except for the R_{max} value within the city of Aachen that was derived from a Famennian rock outcrop which is too small to be shown on the map (Babinecz, 1962; Teichmüller and Teichmüller, 1979; von Winterfeld, 1994). The triangular symbol marks the position of the RWTH-1 drill-hole in the north of Aachen and to the north of the Aachen-Midi thrust which is here named Aachen thrust. The Aachen imbrication zone and the Inde syncline form the northernmost structures of the Venn-Weser-Inde nappe mentioned in the text.

Using numerical modeling, Lünenschloss *et al.* (1997) and Lünenschloss (1998) explained the regional distribution of vitrinite reflectance in the Wurm syncline and pointed out that under realistic burial depths of 4.5 km (Rottke and Stroink, 1999), significant fluid discharge in the footwall of the Aachen thrust is required. According to this model, paleotemperatures between 210 and 310ºC can be assumed for the rock units of the RWTH-1 drill-hole. A recent study of fluid inclusions, calcite-dolomite equilibria and chlorite composition of samples from the RWTH-1 drill core (Lögering *et al.*, 2006), indicates temperatures of 280−370ºC for minerals formed in the veins which are characteristic of the upper core section. High temperatures and low salinities of fluids (<9 wt.%) are considered similar to those of Variscan tectonic brines described by Behr *et al.* (1993) (Lögering *et al.*, 2006).

In post-Variscan times the region was affected by Pb-Zn mineralization at temperatures below 150ºC which was also controlled by major fracture zones (Muchez *et al.*, 1994; Friedrich *et al.*, 1993). For the Pb-Zn deposit of Mechernich (Germany) Schneider *et al.* (1999) derived a Jurassic age of 168±6 Ma.

SAMPLES AND METHODS

Sample preparation

Samples exclusively from drill-cores were used except for three samples from cuttings (Table 1), which were taken for testing methods and for compar-

Table 1. Description of RWTH-1 samples, mineral composition in the order of modal abundance in whole rock, and structural information for the <2 μm fraction.

Sample	Depth (m)	Lithology	Mineral composition, wr	*d* value Il (005) Å	CIS (illite 001)	CIS (chlorite 002)	Wt.% of serpentine in chlorite*
158	190.20	shale	Qz, Chl, Wm, Fsp	2.0010	0.61	0.33	7.3
18-2	1438.00	slate	Qz, Wm, Chl	2.0014	0.52	0.34	11.2
18-3	1439.40	slate	Qz, Chl, Wm	n.d.	0.50	0.33	10.2
20-3	1444.70	slate	Qz, Chl, Wm, Cc	n.d.	0.58	0.35	12.6
25-16	1457.40	siltstone	Qz, Wm, Chl, Hm, Dol	2.0036	0.50	0.31	9.5
1860red	1936.10	slate	Qz, Chl, Wm, Hm	2.0014	0.59	0.31	5.4
1860grn	1936.10	slate	Qz, Chl, Wm	2.0007	0.50	0.29	4.2
52-1	2141.40	shale	Qz, Chl, Wm, Fsp	2.0007	0.46	0.26	3.2
54-1	2537.70	shale	Qz, Chl, Wm, Fsp, Cc	n.d.	0.46	0.31	6.7
59-1	2542.00	shale	Qz, Fsp, Chl, Wm, Cc	2.0013	0.45	0.28	9.7

Abbreviations: Cc = calcite, Chl = chlorite, Dol = dolomite, Fsp = feldspar, Hm = hematite, Il = illite, Qz = quartz, Wm = white mica, wr = whole rock, n.d. = not determined.
Samples 158, 1860red and 1860grn are from cuttings.
Samples 18-2, 18-3, 20-3, 25-16 are from the first core interval.
Samples 52-1 represent the second and 54-1, 59-1 the third core intervals.
* Maximum abundance of serpentine in chlorite (wt.%) based on Newmod® calculation of $w(001_{chlorite}) - w(004_{chlorite})$

ison purposes. To prepare the <2 μm fraction, only rock pieces without macroscopically visible veins or chlorite-filled planes were selected.

Samples were washed and carefully crushed and ground under water in a mortar mill for 5 min under constant machine parameters thus minimizing and keeping constant, preparation effects on crystallinity (Krumm, 1992). The <2 μm fraction was obtained by settling after Sr saturation according to Eberl *et al.* (1987). From the clay fractions, ~200 mg were dispersed in 2 mL of H_2O and transferred to glass slides measuring 28 mm × 48 mm. Preliminary measurements showed that the reproducibility at sample loadings of <10 mg/cm^2 were not satisfactory (Etoundi, 2006). Therefore, loading of 15 mg/cm^2 was chosen, which yields samples infinitely thick to the X-ray radiation.

X-ray diffraction and interpretation of peak-profile shapes

The air-dried specimens were scanned from 2 to 35º2θ and from 47 to 61º2θ (for 005 illite) in steps of 0.015º2θ using filtered CoKα radiation. The Huber 423 goniometer (r = 223 mm) was equipped with two Soller slits with an axial divergence of <0.5º. The divergence slits were set to values where beam overflow had no influence on the peak shape. Polytype determination of illite was performed on the randomly distributed material of the <2 μm fraction using a Guinier image plate camera (Huber G670). The scans were fitted with MacClayFit (Stanjek and Häusler, 2000).

Interpretations of peak parameters in terms of 'crystallinity', 'particle size' or 'strain' have to be done with caution because the observed profile, h, is actually the convolution of the pure diffraction profile, f, of the sample with the profile of the instrument, g. Although the extraction of f is possible using Stoke's method (Klug and Alexander, 1974), the pure diffraction profile, f, is itself the fold of several diffraction effects. The most important contribution to the integral breadth (w) of the profile f stems from an average coherence length, which is frequently identified as being similar or even equal to the apparent particle size perpendicular to the reflecting planes (*e.g.* Guinier, 1963). The profile shape of such a pure size-broadened sample has contributions from both Lorentzian and Gaussian profiles, which make up the Voigt profile (Langford and Wilson, 1978). In preliminary evaluations we used the numerical approximation to the Voigt profile as given by Thompson, Cox and Hastings (Thompson *et al*., 1987) for extracting the Gaussian and Lorentzian contributions to the 00*l* peaks. Non-systematic variations of both parameters rendered this approach inapplicable. Consequently, for the present study the Pseudo-Voigt function was used for illite and the integral peak breadths were interpreted without considering the profile shape.

The chlorite peaks were fitted with a Pseudo-Voigt function, whereas the two quartz peaks (which served as an internal standard) were modeled with a Thompson-Cox-Hastings function using the *X* (Scherrer broadening) and the *W* parameter (Gaussian component). The latter function couples the peak breadths of the 100 and the 101 peaks and enabled the separation of the illite 003 peak from the 101 of quartz. The goodness-of-fit ranged between 1.06 and 1.48.

Apart from a volume-averaged particle size, the kind and dispersion of the particle-size distribution affects the profile shape (Rao and Houska, 1986; Langford *et al*., 2000) and the particle shape in turn changes the profile shape and may yield anisotropic peak broadening (Scherrer, 1918; Langford and Wilson, 1978). Further contributions to the profile shape come from mixed layering and from stacking faults which, however, would only affect *hk*0 reflections (Mering, 1949). The latter are not measured in textured samples used here. The contribution of strain to the profile shape can principally be assessed by the method of Bertaut (1950), but requires Fourier analyses and, hence, reference samples which yield the instrumental profile, *g*. Consequently, it is evident that for a study that is not based on Fourier deconvolution, even the evaluation of four to five 00*l* peaks does not allow us to quantify the contribution of strain. As the most important contribution to the peak breadth is given by the average coherence length, the integral breadths, *w*, of illite and chlorite are considered to primarily reflect crystal thickness (*i.e.* 'crystallinity').

Since glycolation of samples did not give peak widths significantly different from air-dried samples (Etoundi, 2006), we report here only results from air-dried specimens.

Standardization procedures

For standardization to the 'crystallinity' index standard (CIS) according to Warr and Rice (1994), repeated analyses of the standards SW1 to SW6 resulted in the conversion equations:

$$CIS_{illite\ 001} = w_{uncalibrated} * 1.147 + 0.050,\ R^2 = 0.92$$
$$CIS_{chlorite\ 002} = w_{uncalibrated} * 1.004 + 0.080,\ R^2 = 0.96$$

Thus, effects caused by sample and slide preparation and also by using Co instead of Cu radiation are eliminated. Four true replicates of sample 158 (including rock-sample preparation, glass-slide production and XRD analysis) yielded a precision for the $CIS_{illite\ 001}$ and $CIS_{chlorite\ 002}$ of 0.028º and 0.023º (1σ), respectively. For *d* values, a precision of 0.003º was obtained. For simplicity and in order to mark the standardized character of the data, the established abbreviation 'CIS' (crystallinity index standard, Warr and Rice, 1994) and the term 'crystallinity' are used here though the one-dimensional XRD data are not suitable to define the 'crystallinity' of a three-dimensional structure (Guggenheim *et al.*, 2002).

Chemical analyses and IR spectrometry

The K concentration of the <2 μm fraction was obtained using HF-H_3BO_4 dissolution in a microwave equipped with Teflon bombs and quantitative determination by inductively coupled plasma-optical emission spectroscopy (Perkin Elmer DV 2000). Nitrogen analysis of the <2 μm fraction was performed in the 'Zentralabteilung für Chemische Analysen', Forschungszentrum Jülich (analyst M. Michulitz) on a TC436Ar (Leco) analyzer with a thermal conductivity detector at T_{max} = 2700ºC with He as the carrier gas. Determination of C_{org} was carried out using a RC-412 (Leco) analyzer at T < 500ºC with oxygen gas. CO_2 produced by combustion was detected by infrared (IR) absorption. The precision of both methods is better than 4%. The IR absorption spectra were measured with a resolution of 2 cm^{-1} on a Perkin Elmer 1600 FTIR spectrometer using discs made of 200 mg NaCl and 1 mg of sample. The sample material was decarbonated with 0.5 N HCl and oxidized using H_2O_2 (15%) in order to eliminate organic matter.

RESULTS

The samples are slates and shales mainly composed of quartz, illite, chlorite and in some cases also hematite and calcite or dolomite (Table 1, Figure 2). Feldspar is a minor constituent in samples 158, 52-1, 54-1 and 59-1 (Table 1). Based on the 002 reflections of microcline and albite in the whole-rock samples, one can assume that albite is more abundant than K-feldspar. This is in line with the results of Flehmig (1983) who found that in Upper Devonian shales and silty shales of the Rhenohercynian, albite is generally at least twice as abundant as K-feldspar. Calcareous microfossils show stylolite planes indicative of pressure solution (sample 20-3).

Quartz grains show pressure solution creep with quartz overgrowth in strain shadows. Samples 18-2, 18-3 and 20-3 are locally deformed by cataclasis with transgranular fractures and grain-size reduction, in which the quartz grains locally expose dislocation glide deformation as shown by undulose extinction (Figure 2b). The transgranular fractures are filled by calcite. Quartz veins are blocky to elongate blocky and partly recrystallized by subgrain rotation and grain-boundary migration recrystallization. These features point to intensive deformation within a fault zone in the upper core section (1392−1515 m). Samples 18-2, 18-3, 20-3 are strongly cleaved and, locally, the S1 cleavage is overprinted by a second set of cleavage planes (S2, Figure 2a). Cleavage S2 is oriented oblique to S1 indicating shear deformation. Chlorite which is characterized by greenish-blue anomalous interference colours indicative of an Fe-rich variety (Deer *et al.*, 1992) also occurs in fine sheets and veins. It is the dominant mineral in cleavage planes and veins where it

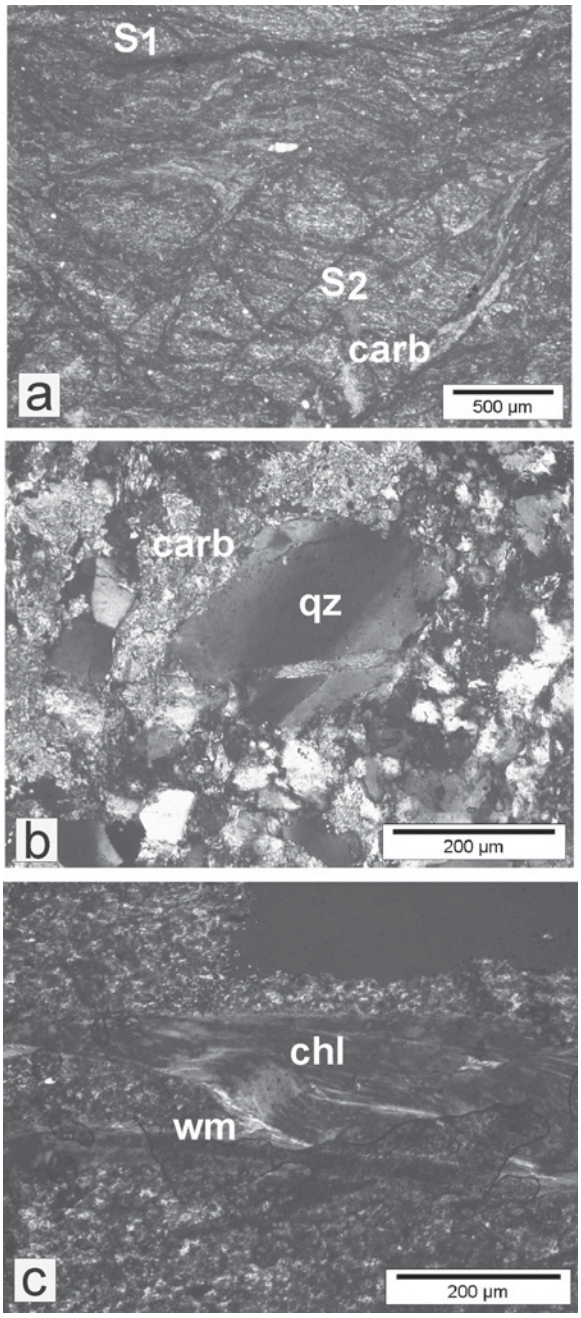

Figure 2. Thin-sections of representative samples from the upper core section of the RWTH-1 drill-hole, under crossed polars: (a) sample 18-2, S1 and S2 are cleavage planes with chlorite, carbonates (carb) form irregular patches which are sub-parallel to S2 as well as irregularly distributed; (b) sample 18-2, undulose extinction of detrital quartz (qz), carbonates are marked by carb, lower half of the photo predominantly shows detrital quartz; (c) sample 18-3, undulose extinction in folded platy chlorite (chl), light gray flakes are white micas (wm) formed in chlorite.

is associated with quartz giving evidence for a fluid and strain-controlled crystallization of chlorite. Chlorite overgrows calcite veins, implying formation after calcite-vein generation. Within cleavage planes, chlorite crystals are partly bent and show undulose extinction. White mica occurs in the matrix as detrital grains and sometimes formed in extension cracks between chlorite crystals in cleavage planes and chlorite veins (Figure 2c). These white micas which are only found in sample 20-3 crystallized during deformation along the cleavage planes with sizes up to 100 µm (Figure 2c).

Shaley rocks (*i.e.* samples 158, 52-1, 54-1, 59-1) and siltstone sample 25-16 contain chlorite veinlets associated with quartz veins. The presence of chlorite veins underlines the hydrothermal formation of chlorite in these rocks, too.

Illite and chlorite, structural information

The results of the XRD analyses on textured slides are presented in Table 1 and in Figures 3 and 4. Analysis of the randomly oriented samples (<2 µm fraction) indicates that illites belong to the $2M_1$ polytype. The $w(001_{illite})$ decreased only slightly when the samples were treated with ethylene glycol. This indicates that the number of swelling layers is very small or non-existent, though small amounts of smectite have to be expected in order to explain the variation of $w(00l_{illite})$ (Figure 3a). The d values for the illite 005 reflection of all samples vary between 2.0007 and 2.0036 Å (Table 1).

Taking into consideration that a representative d_{005} value for a $2M_1$ white mica is 2.00148 Å (Brindley, 1980) one can state that, within the precision of the method (here 0.003 Å), the d_{005} values of illite in the samples are identical to this value. As $hk0$ reflections cannot be determined in oriented specimens, the data do not allow us to discuss possible stacking defects which may be caused by deformation (Merriman and Peacor, 1999). However, significant structural distortion would lead to a positive correlation of $w(00l_{illite})$ and tan(θ) (*i.e.* increasing order of the reflection) which cannot be observed (Figure 3a).

The basal reflections of chlorite (<2 µm fraction) in all samples show a similar pattern (Figure 3b) to those of illite (Figure 3a). The $w(00l_{chlorite})$ values vary around a constant value and do not increase significantly with increasing order. This precludes significant structural distortion which could be expected considering the bent sheets of chlorite showing undulose extinction (Figure 2). The variation of the $w(00l_{chlorite})$ indicates the presence of serpentine layers within chlorite (Reynolds *et al.*, 1992). A Newmod® simulation (Table 1) on the basis of the ratios of $w(001_{chlorite})$ to $w(004_{chlorite})$ points to serpentine abundances of up to 12.6 wt.% within chlorite (Table 1).

Illite and chlorite grades

$CIS_{illite\ 001}$ ranges from 0.45 to 0.61 with the highest values (*i.e.* lowest grade) in the cuttings and the lowest values in the lowermost drill-core sample (Table 1,

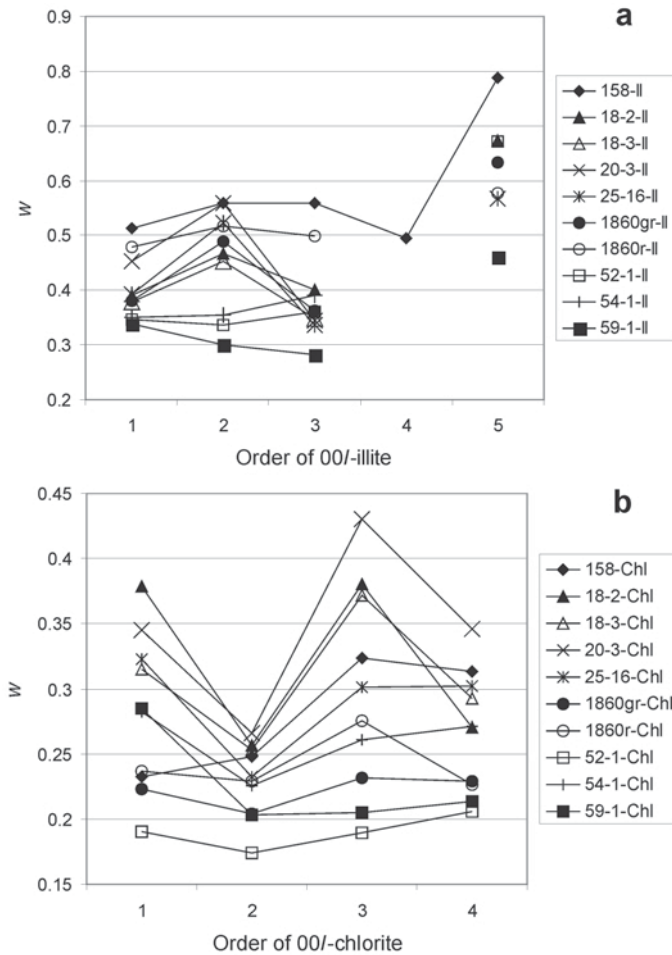

Figure 3. Integral breadth (*w*) in º2θ (CoKα) of basal reflections of illite (a) and chlorite (b) in <2 μm fractions. Integral breadths were multiplied by cos(θ) in order to account for Scherrer broadening.

Figure 4). The zone of the upper-core section, which is characterized by intensive deformation and vein formation, shows varying $CIS_{illite\ 001}$ values. However, within the limits of precision, all illite data overlap to a large extent. Taking the $CIS_{illite\ 001}$ values and the absence or presence of only small proportions of interlayered smectite into account, the illite data of all RWTH-1 samples would indicate late diagenetic grade (Merriman and Peacor, 1999) over the whole drill-core.

In contrast to the $CIS_{illite\ 001}$, the $CIS_{chlorite\ 002}$ of chlorite points to anchizonal grades in the lower-core sections (average of $CIS_{chlorite\ 002}$ = 0.28) whereas the upper-core section shows diagenetic grade for chlorite (average of $CIS_{chlorite\ 002}$ = 0.33, Figure 4). Most data show a large overlap within the limits of precision.

Ammonium in illite

Ammonium-rich clay minerals have often been described and are supposed to affect determination of illite 'crystallinity' (Árkai *et al.*, 2004, and references therein). In sedimentary settings, NH_4, probably derived from maturing organic matter, may be adsorbed on clay mineral surfaces or it substitutes for K in the interlayer position (*e.g.* Williams *et al.*, 1989; Šucha *et al.*, 1998). Nieto (2002) showed that either K or NH_4 predominate in distinct packets of dioctahedral illite clay minerals or white mica. The NH_4-rich illite component is called tobelite after the Tobe mine (Higashi, 1982 in Árkai *et al.*, 2004).

Krooss *et al.* (2005) pointed out that significant amounts of inorganic NH_4 exist in Carboniferous shales of the North German Basin and Mingram *et al.* (2005) found that 50−100% of N in this basin is fixed as NH_4 in inorganic phases. This and the potential role of NH_4 for illite 'crystallinity' necessitated NH_4 determination in the samples studied here in those cases in which enough of the limited drill core material was available. Nitrogen in the <2 μm fraction can be present in organic phases and as NH_4 in K-bearing minerals such as illite. In order to distinguish between organic and inorganic N the total organic carbon concentration (TOC) and the N/C ratio in the organic phases have to be known (Árkai *et al.*, 2004). Krooss *et al.* (2005) determined N/C ratios from kerogen of Paleozoic rocks of the North German Basin which range between 0.006 and 0.016 (by weight).

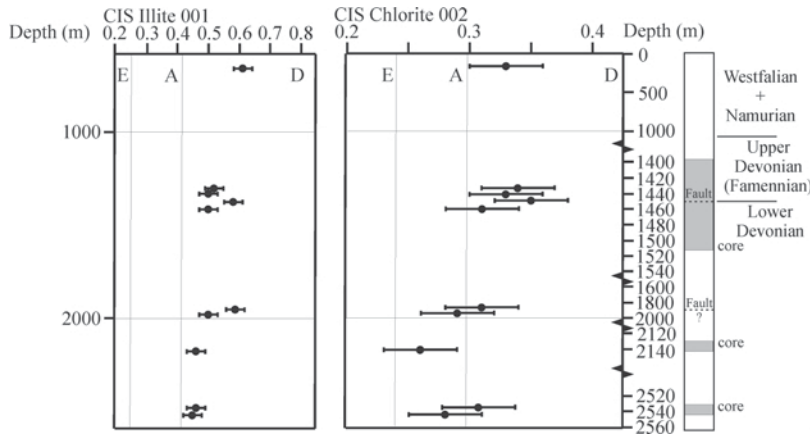

Figure 4. CIS values *vs.* depth of the RWTH-1 drill-hole. Gray fields on the right side mark core sections; depth not to scale. E, A and D denote epizone, anchizone and diagenetic zones, respectively. Limiting values for illite by Kübler (1968, 1990) and for chlorite by Árkai *et al.* (1996). Stratigraphic information according to Österreich *et al.* (2005).

The K_2O concentration of the <2 μm fractions (Table 2, samples 158, 20-3, 25-16) which consist of illite, chlorite and quartz can be used to quantify the amount of illite (wt.%) because this is the predominant K-bearing phase. As K-feldspar, another K-bearing mineral, was detected by XRD as being only a minor constituent in the whole-rock fraction of sample 158 (Table 1), and even less common in the <2 μm fraction, K-feldspar is considered as insignificant here. For this calculation, a K_2O concentration of 7.6% was assumed for the illite according to Środoń *et al*. (1986).

After assessment of the illite abundance and calculation of the minimum and maximum amounts of inorganic N derived from N/TOC ratios mentioned above (Krooss *et al.*, 2005), considered to be entirely incorporated in illite (not in chlorite or quartz), one can estimate the NH_4 amounts in illite (Table 2) which range between 0.19 and 0.44 wt.%. As the <2 μm fraction was Sr saturated, NH_4 is considered to be situated in interlayer position rather than being adsorbed on the surface. On the basis of the sum of N + K, the molar proportion of NH_4 in illite would range between 11.8 and 27.4%. However, such NH_4 concentrations should lead to a shift in the basal reflection towards higher *d* values (Árkai *et al,.* 2004; Drits *et al*., 1997). Assuming a linear increase of the *d* value with increasing NH_4, at least for small amounts of NH_4 and independent of the distribution of NH_4 (Drits *et al*., 1997), and that the pure NH_4-illite (*i.e.* tobelite) has a *d* value of 2.048 Å (Árkai *et al,.* 2004), a molar NH_4 abundance of 15% should result in a d_{005} value of 2.0085 Å. This is beyond the limits of precision (0.003 Å) greater than the maximum *d* value of 2.0036 Å (Table 1) in the illites of the RWTH-1 drill core and thus points to NH_4 abundance in illite of <15%. Fourier transform infrared (FTIR) absorption spectra of the <2 μm fractions confirm this result. These show the characteristic absorption near 1430 cm^{-1} indicative of NH_4 in phyllosilicates whereas absorption between 2800 and 3300 cm^{-1} caused by N–H stretching (Wilson *et al*., 1992; Pironon *et al*., 2003) is not pronounced. If compared to absorption spectra of smectite saturated in solutions of various NH_4/K ratios, the sizes of the absorbance peaks near 1430 cm^{-1} of the <2 μm fractions are consistent with NH_4 abundance in illite <15%. It is possible that the NH_4 concentrations in illite derived from the chemical analyses are too high as they are based on the assumption of N/TOC ratios in kerogen similar to characteristic ratios in the North German Basin (Krooss *et al*., 2005). The N/TOC ratio in kerogen may be greater in the rocks of the RWTH-1 drill core.

Table 2. Total organic carbon (TOC), N and K_2O concentrations in the <2 μm fractions of the RWTH-1 samples and calculated illite abundance* and NH_4 concentration in illite. All data in wt.%. See text for further explanation.

Sample	Lithology	TOC	N	K_2O	Illite*	NH_4 **	NH_4 ***
158 I	Shale	1.55	0.144	3.04	40.0	0.36	0.44
20-3	Slate	0.36	0.101	3.75	49.0	0.19	0.21
25-16	Siltstone	0.38	0.31	3.71	48.8	0.25	0.26

* based on the assumption of 7.6 wt.% K_2O in illite (Środoń *et al*., 1986)
** based on N/TOC = 0.02
*** based on N/TOC = 0.005

DISCUSSION

In the samples studied here, hydrothermal syntectonic crystallization of chlorite and white mica (sample 20-3) can be observed. Quartz in cataclastic fault zones exhibits discontinuous undulose extinction and quartz in veins shows grain boundary migration/sub grain rotation recrystallization. Such features point to minimum temperatures of 200−250ºC (Oncken, 1989) for the hydrothermal event represented in the RWTH-1 drill core. This is in agreement with homogenization temperatures of up to 370ºC in veins (Lögering *et al*., 2006). The temperatures of the hydrothermal event are greater than those derived by paleogeothermometers of the host-rock in the foreland of the frontal Variscan thrust of ~200ºC (Hollmann, 1997; Rottke and Stroink, 1999). This supports previous assumptions that hydrothermal fluid flow was necessary to explain the high coalification grades close to the Aachen thrust (von Winterfeld, 1994; Lünenschloss *et al*., 1997; Lünenschloss, 1998). As was indicated by Knapp (1980), maturation of organic material and therefore also the hydrothermal event discussed here is of Carboniferous and thus Variscan age. The fluids have characteristic features (*i.e.* temperature, salinity) of tectonic brines (Lögering *et al*., 2006, Behr *et al*., 1993) which also point to the Variscan event. The alternative − that the hydrothermal event is post-Variscan − is less plausible because post-Variscan mineralization occurred at temperatures predominantly <150ºC (Muchez *et al*., 1994; Friedrich *et al*., 1993; Redecke, 1992) and caused the formation of Pb-Zn-sulfides which are absent from the RWTH-1 drill core (Chatziliadou *et al*., 2005; Lögering *et al*., 2005).

Thrusting and thrust loading, as can be expected within the orogenic wedge to the south of the Aachen thrust during the Variscan orogeny, caused fluid expulsion into the foreland (Oliver, 1986; Moore, 1989; von Winterfeld, 1994) and fluid-overpressure formation above and below the thrust plane, if the bulk rock is of intermediate permeability (Smith and Wiltschko, 1996). In our field area, both hangingwall and footwall consist of shale-sandstone multilayers and thus have the potential to keep fluid pressures high over the time-interval of the events discussed here. Ge and Garven (1992) numerically simulated the fluid expulsion associated with thrust loading and calculated a disturbance of the fluid flow field. They proposed that fluid expulsion towards the foreland takes ~5000 y before returning to normal hydrological conditions. The injection of hot fluids would thus increase the temperature in the host-rock adjacent to the Aachen thrust during a period of 5000 y.

Illite

In contrast to the thermal indicators (*i.e.* mineralogical observations of the RWTH-1 drill core, published vitrinite and fluid inclusion data) mentioned above, the CIS_{illite} data reflect a late diagenetic grade and thus temperatures approaching <200ºC.

A lower grade of illite relative to chlorite and other grade indicators is common and discussed frequently (Árkai *et al*., 2004; Maynard *et al*., 2001; Wang *et al*., 1996). It can be ascribed to a retarded reaction progress of illite which is due to isolation of phyllosilicates from porefluids (*i.e.* low water/rock ratio, Pollastro, 1993) caused by precipitation of secondary minerals (Árkai *et al*., 2004). Also, low K activity and high H_2O pressure slow down the smectite-illite reaction (Árkai *et al*., 2004; Pollastro, 1993). The concentration of K_2O in the rocks of RWTH-1 drill-hole varies between 1.38 and 4.81 wt.% depending on the amount of detrital white mica, clay minerals and minor detrital K-feldspar (Sindern, unpublished data). It is therefore assumed that K should have been present in a porefluid. Ammonium substitutes for K in the illite structure to <15% and is therefore also considered less significant as a reason for decreasing the growth rate of illite.

As was pointed out in the method section above, the XRD profile from textured samples mainly reflects crystallite size but cannot be used to quantify structural distortion unless extensive corrections are applied to the peak profiles. If deformation in the rocks of the RWTH-1 drill-hole had a significant impact on the illite structure leading to the high integral breadth *w*, as was described by Árkai *et al*. (1997) for rocks in the hangingwall of the Glarus thrust in Switzerland (Merriman and Frey, 1999), this should be reflected in our samples here because the different core intervals show different degrees of deformation. In this case one would expect that CIS values from the slate samples mainly of the first core interval would be greater than those of shale and siltstone samples. A comparison of the average $CIS_{illite\ 001}$ of the more intensively deformed samples (0.54±0.04 SD) with the average $CIS_{illite\ 001}$ of the less deformed samples (0.50 ± 0.07 SD) (Table 1, Figure 4) makes clear that deformation does not have a significant impact on the $CIS_{illite\ 001}$.

In the samples studied here, illite is almost entirely restricted to the rock matrix whereas chlorite occurs in veins, attesting to the role of fluids especially in the formation of chlorite. Crystal growth of chlorite was therefore probably faster than growth of illite within the less permeable matrix. This explains why in some cases $CIS_{chlorite}$ indicates higher grades than CIS_{illite} (Figure 4). Transfer of elements during the (hydro-) thermal peak and thus illite growth was restricted because the duration of the event was too short for the permeability conditions in the rock. The late diagenetic grade reflected by illite is equivalent to the temperatures reported for the foreland of the Aachen thrust (200ºC, Hollmann, 1997; Rottke and Stroink, 1999, Fielitz and Mansy, 1999). As the illite of the RWTH-1 drill core seems unaffected by the hydrothermal event, it is therefore concluded that illite mirrors the burial history rather than hydrothermal fluid flow.

Chlorite

$CIS_{chlorite}$ data reflect a late diagenetic grade in the upper-core section and in part, anchizonal grade, in the lower-core sections (Figure 4). Chlorite which occurs in veins and cleavage planes should reflect the higher grade estimated for the hydrothermal event from the mineralogical observation. The deviation to lower $CIS_{chlorite}$ grades than expected could be explained by deformation of chlorite. However, the integral breadths, w, of the basal reflections do not increase with increasing order of $00l_{chlorite}$ and thus are not consistent with structure deformation being dominant (Figure 3b). This suggests that the XRD data do not reflect post-crystalline deformation. As the partly oriented structure and undulose extinction of chlorite indicate deformation effects, hydrothermal chlorite growth must have occurred syntectonically. Syntectonic hydrothermal growth of platy and fibrous chlorite occurred by incipient nucleation along the tips and edges of crystals. This probably limited domain size and thus also the integral breadth of the basal reflection. It would also explain why the chlorite precipitated at higher (up to epizonal) temperatures yields lower grades indicated by $CIS_{chlorite\ 002}$ values (*i.e.* diagenetic to anchizonal). Similar to the results derived from investigation of illite, one has to assume here, too, that the anchi- to epizonal peak thermal conditions did not last long, as otherwise one would expect domain growth under such conditions.

The finding of increased supermature R_{max} values along the Aachen thrust supports the probability of a short-duration hydrothermal event. Vitrinite matures faster and its maturation is not as dependent on fluid-rock interaction as the growth of illite and chlorite (Velde and Lanson, 1993). Furthermore, in rocks in which chlorite and K-bearing phases such as illite next to detrital white mica and K-feldspar in some cases are as abundant, as in the samples studied here (Table 1), one would expect the formation of biotite (Inoue, 1995) if temperatures reached 300ºC. As temperatures were as high as, or greater than 300ºC, the lack of biotite points to a hydrothermal event which was too short for its growth.

CONCLUSIONS

Investigation of material from three core sections of the RWTH-1 drill-hole in Aachen shows mineralogical and structural evidence of intensive Carboniferous (Variscan) hydrothermal activity in the footwall of the Aachen thrust. Mineral and microstructural data indicate minimum temperatures of 200–250ºC, though maximum temperatures of the hydrothermal event up to 370ºC can be expected taking recently published data for comparison. $CIS_{illite\ 001}$ values of 0.45–0.61 (Δº2θ) and insignificant amounts of smectite indicate a late diagenetic grade for illite, pointing to temperatures of <200ºC. Illite which contains minor amounts (<15 mole %) of NH_4 substituting for K is neither significantly affected by deformation nor by the hydrothermal impact but mirrors the burial history of the Wurm syncline. Chlorite, mainly formed in veins and cleavage planes, has $CIS_{chlorite\ 002}$ values between 0.35 and 0.26 (Δº2θ) which only partly point to anchizonal grade. However, chlorite grew syntectonically as is shown by bent and predominantly stretched laths which do not have deformed structures. The evidence of syntectonic hydrothermal activity is in line with the idea that hydrothermal fluid flow was caused by fluid expulsion along the Aachen thrust due to thrusting and thrust loading during the Variscan orogeny. Syntectonic hydrothermal chlorite growth by incipient nucleation along crystal edges limited domain size and thus also the $CIS_{chlorite\ 002}$ values. The lack of larger chlorite domains indicates that the hydrothermal event, while probably reaching epizonal temperatures, did not last long enough to allow further crystal growth of chlorite and did not generate biotite. Based on numerical simulations in similar settings, one can assume a duration of ~5000 y for the expulsion of tectonic brines along the Aachen thrust which is part of the frontal Variscan front.

ACKNOWLEDGMENTS

This study was funded by DFG grant SI 810/2-1. The work of S. Prantl who helped with the figures, of G. Siebel and J. Warnsloh who supported XRD analyses, and of Chr. Marchel and V. Havenith (all in Aachen), who assisted with FTIR spectroscopy and TOC analyses, respectively, is gratefully acknowledged. Lars Reuning (Aachen) helped to identify calcareous microfossils in one sample. We also thank R.J. Merriman, N. Liewig and R.E. Ferrell, Jr. for their constructive reviews which helped significantly to improve the manuscript.

REFERENCES

Árkai, P., Merriman, R.J., Roberts, B., Peacor, D. and Tóth, M. (1996) Crystallinity, crystallite size and lattice strain of illite, muscovite and chlorite: comparison of XRD and TEM data for diagenetic to epizonal pelites. *European Journal of Mineralogy*, **8**, 1119–1137.

Árkai, P., Balogh, K. and Frey, M. (1997) The effects of tectonic strain on crystallinity, apparent mean crystallite size and lattice strain of phyllosilicates in low temperature metamorphic rocks. A case study from the Glarus overthrust, Sitzerland. *Schweizerische Mineralogische und Petrographische Mitteilungen*, **77**, 27–40.

Árkai, P., Livi, K.J.T., Frey, M., Brukner-Wein, A. and Sajgo, C. (2004) White micas with mixed interlayer occupancy: a possible cause of pitfalls in applying illite Kübler index ('crystallinity') for the determination of metamorphic grade. *European Journal of Mineralogy*, **16**, 469–482.

Babinecz, W. (1962) Das Inkohlungsbild des Aachener Steinkohlengebirges, dargestellt im Niveau des Flözes Großlangenberg. *Forschritte Geologie Rheinland und Westfalen*, **3**, 679–686.

Battaglia, S., Leoni, L. and Sartori, F. (2004) The Kübler index in late diagenetic to low-grade metamorphic pelites: A critical comparison of data from 10 Å and 5 Å peaks. *Clays and Clay Minerals*, **52**, 85–105.

Behr, H.J., Gerler, J., Hein, U.F. and Reutel, C.J. (1993)

Tectonic brines und basement brines in den mitteleuropäischen Varisziden: Herkunft, metallogenetische Bedeutung und geologische Aktivität. *Göttinger Arbeiten zur Geologie und Paläontologie*, **58**, 3–28.

Bertaut, E.F. (1950) Raies de Debye-Scherrer et répartition des dimensions des domaines de Bragg dans les poudres polycristallines. *Acta Crystallographica*, **3**, 14–18.

Brindley, G.W. (1980) Order-disorder in clay mineral structures. Pp. 125–196 in: *Crystal Structures of Clay Minerals and their X-ray Identification* (G.W. Brindley and G. Brown, editors). Monograph No. **5**, Mineralogical Society, London.

Chatziliadou, M., Sindern, S., Hilgers, C. and Kramm, U. (2005) Spurenelementverteilung in Gesteinen der RWTH-1 Bohrung, Aachen. *Berichte der Deutschen Mineralogischen Gesellschaft*, *Beih. Z. European Journal of Mineralogy*, **17**, 22.

Clauer, N., Liewig, N., Pierret, M.-C. and Toulkeridis, T. (2003) Crystallization conditions of fundamental particles from mixed-layer illite-smectite of bentonites based on isotopic data (K-Ar, Rb-Sr and $\delta^{18}O$. *Clays and Clay Minerals*, **51**, 664–674.

Deer, W.A., Howie, R.A. and Zussmann, J. (1992) *An Introduction to the Rock-forming Minerals*, 2nd edition. Longman, Essex, UK, 696 pp.

Drits, V.A., Lindgreen, H. and Salyn, A.L. (1997) Determination of the content and distribution of fixed ammonium in illite-smectite by X-ray diffraction: Application to North Sea illite-smectite. *American Mineralogist*, **82**, 79–87.

Eberl, D.D. and Velde, B. (1989) Beyond the Kübler index. *Clay Minerals*, **24**, 571–577.

Eberl, D.D., Środoń, J., Lee, M., Nadeau, P.H. and Northrop, H.R. (1987) Sericite from the Silverton caldera, Colorado: correlation among structure, composition, origin, and particle size. *American Mineralogist*, **72**, 914–934.

Essene, E.J. and Peacor, D.R. (1995) Clay mineral thermometry – a critical perspective. *Clays and Clay Minerals*, **43**, 540–553.

Etoundi, Y. (2006) Tonmineralogische Untersuchung an Material der RWTH-1 Bohrung. Diploma thesis, Institute of Mineralogy and Economic Geology, RWTH Aachen University, Gernmany, 61 pp.

Fielitz, W. and Mansy, J.L. (1999) Pre- and synorogenic burial metamorphism in the Ardenne and neighbouring areas (Rhenohercynian zone, central European Variscides). *Tectonophysics*, **309**, 227–256.

Flehmig, W. (1983) Mineral composition of pelitic sediments in the Rhenohercynian zone. Pp 257–265 in: *Intracontinental Fold Belts* (H. Martin and F.W. Eder, editors). Springer Verlag, Berlin, Heidelberg, New York.

Friedrich, G., Germann, A. and Jochum, J. (1993) Schichtgebundene Pb-Zn-Vorkommen in klastischen Sedimenten vom Typ Maubach-Mechernich – Lagerstättenbildung durch intraformationale Prozesse. *Mitteilungen der Österreichischen Mineralogischen Gesellschaft*, **138**, 93–106.

Ge, S. and Garven, G (1992) Hydromechanical modeling of tectonically driven groundwater flow with application to the Arkoma foreland basin. *Journal of Geophysical Research*, **97**, 9119–9144.

Glasmacher, U.A. (1995) Variszische und postvariszische Fluidsysteme. Pp 1–40 in: *KW-relevante Eigenschaften potentieller Mutter- und Speichergesteine am Nordrand des Linksrheinischen Schiefergebirges* (R. Walter, U. Glasmacher and M. Wolf, editors). RWTH-Aachen, BMBF Forschungsprojekt 032 6804 A 5, Teil 5.

Glasmacher, U.A., Tschernoster, R., Clauer, N. and Spaeth, G. (2001) K-Ar dating of magmatic sericite crystallites for determination of cooling paths of metamorphic overprints. *Chemical Geology*, **175**, 673–687.

Guggenheim, S., Bain, D.C., Bergaya, F., Brigatti, M.F., Drits, V.A., Eberl, D.D., Formoso, M.L.L., Galán, E., Merriman, R.J., Peacor, D.R., Stanjek, H. and Watanabe, T. (2002) Report of the Association Internationale pour l'Etude des Argiles (AIPEA) Nomenclature committee for 2001: Order, disorder and crystallinity in phyllosilicates and the use of the 'Crystallinity Index'. *Clay Minerals*, **37**, 389–393.

Guinier, A. (1963) *X-ray Diffraction in Crystals, Imperfect Crystals and Amorphous Bodies*. Freeman and Company, San Francisco, USA, 387 pp.

Higashi, S. (1982) Tobelite, a new ammonium dioctahedral mica. *Mineralogical Journal*, **11**, 138–146.

Hilgers, C., Büker, C. and Urai, J.L. (2006) Fossil overpressure compartments? A case study from the Eifel area and some general aspects. In: *TSK (Symposium Tektonik. Strukturgeologie Kristallingeologie) 11* (G. Gudmundsson, editor). Göttingen.

Hollmann, E.G. (1997) Der Variszische Vorlandüberschiebungsgürtel der Ostbelgischen Ardennen – Ein bilanziertes Modell. *Aachener Geowissenschaftliche Beiträge*, **25**, 235 pp.

Hower, J., Eslinger, E.V., Hower, M.E. and Perry, E.A. (1976) Mechanisms of burial metamorphism of argillaceous sediments: Mineralogical and chemical evidence. *Geological Society of America Bulletin*, **87**, 725–737.

Inoue, A. (1995) Formation of clay minerals in hydrothermal environments. Pp. 268–329 in: *Origin and Mineralogy of Clay – Clays and the Environment* (B. Velde, editor). Springer, Berlin.

Jaboyedoff, M., Bussy, F., Kübler, B. and Thelin, Ph. (2001) Illite 'crystallinity' revisited. *Clays and Clay Minerals*, **49**, 156–167.

Kisch, H.J. (1990) Calibration of the anchizone: A critical comparison of illite 'crystallinity' scales used for definition. *Journal of Metamorphic Geology*, **9**, 665–670.

Klug, H.P. and Alexander, L.E. (1974) *X-ray Diffraction Procedures for Polycrystalline and Amorphous Materials*. John Wiley and Sons, New York, 966 pp.

Knapp, G. (1980) *Erläuterungen zur Geologischen Karte der nördlichen Eifel, 1: 100000, 2. Auflage.* Geologisches Landesamt Nordrhein Westfalen, Krefeld, 152 pp.

Krooss, B.M., Friberg, L., Gensterblum, Y., Hollenstein, J., Prinz, D. and Littke, R. (2005) Investigation of the pyrolytic liberation of molecular nitrogen from Palaeozoic sedimentary rocks. *International Journal of Earth Sciences*, **94**, 1023–1038.

Krumm, S. (1992) Illitkristallinität als Indikator schwacher Metamorphose – Methodische Untersuchungen, regionale Anwendungen und Vergleiche mit anderen Parametern. *Erlanger Geologische Abhandlungen*, **120**, 1–75.

Kübler, B. (1964) Les argiles, indicateurs de métamorphisme. *Revue de l'Institut Francais du Petrole*, **19**, 1093–1112.

Kübler, B. (1968) Evaluation quantitative du métamorphisme par la cristallinité de l'illite. *Bulletin du Centre de Recherches de Pau-SNPA*, **2**, 385 –397.

Kübler, B. (1990) "Cristallinité" de l'illite et mixed-layers: brève révision. *Schweizerische Mineralogische und Petrographische Mitteilungen*, **70**, 89–93.

Kübler, B. and Jaboyedoff, M. (2000) Illite crystallinity. *Comptes Rendu de l'Academie Scientifique de Paris, Science de la Terre et des Planètes*, **331**, 75–89.

Langford, J.I. and Wilson, A.J.C. (1978) Scherrer after sixty years: a survey and some new results in the determination of crystallite size. *Journal of Applied Crystallography*, **11**, 102–113

Langford, J.I., Louer, D. and Scardi, P. (2000) Effect of a crystallite size distribution on X-ray diffraction line profiles

and whole-powder-pattern fitting. *Journal of Applied Crystallography*, **33**, 964–974.

Lanson, B. and Kübler, B. (1994) Experimental determination of the coherent scattering domain size distribution of natural mica-like phases with the Warren-Averbach technique. *Clays and Clay Minerals*, **42**, 489–494.

Lögering, M.J., Kolb, J. and Meyer, F.M. (2005) Fluidsysteme in hydrothermalen Gängen der Aachener Geothermie-Bohrung. *Berichte der Deutschen Mineralogischen Gesellschaft, Beih. Z. European Journal of Mineralogy*, **17**, 84.

Lögering, M.J., Kolb, J., Meyer, F.M. and Schwarzbauer, J. (2006) Paläofluide in störungskontrollierten Bruchsystemen der Aachener Geothermie-Bohrung. *Abstract, TSK (Symposium Tektonik, Struktur und Kristallingeologie) 11*, pp. 22–24, März, Göttingen, Germany.

Lundershausen, S., Oesterreich, B., Ribbert, K.H. and Wrede, V. (2005) Geothermal well 'RWTH-1', Aachen – Technical aspects and first geological results. *Abstracts of the Meuse-Rhine Euregio Geologists Meeting: Alden Biesen (Belgian Limbourg)*, 20–21 May 2005.

Lünenschloss, B. (1998) *Modellierung der Temperatur- und Fluidgeschichte an der variszischen Front (Verviers-Synklinorium und Nordeifel)*. Scientific Technical Report STR98/07 Geoforschungszentrum Potsdam, 132 pp.

Lünenschloss, B., Bayer, U. and Muchez, Ph. (1997) Coalification anomalies induced by fluid flow at the Variscan thrust front: a numerical model of the palaeotemperature field. *Geologie en Mijnbouw*, **76**, 271–275.

Maynard, J.B., Elswick, E.R. and Hower, J.C. (2001) Reflectance of dispersed vitrinite in shales hosting Pb-Zn-Cu ore deposits in western Cuba: comparison with clay crystallinity. *International Journal of Coal Geology*, **47**, 161–170.

Mering, J. (1949) L'interférence de rayons X dans les systems a stratification désordonnée. *Acta Crystallographica*, **2**, 371–377.

Merriman, R.J. (2005) Clay minerals and sedimentary basin history. *European Journal of Mineralogy*, **17**, 7–20.

Merriman, R.J. and Frey, M. (1999) Patterns of very low-grade metamorphism in metapelitic rocks. Pp. 61–107 in: *Low-grade Metamorphism* (M. Frey and D. Robinson, editors). Blackwell Sciences, Oxford, UK.

Merriman, R.J. and Peacor, D.R. (1999) Very low-grade metapelites: mineralogy, microfabrics and measuring reaction progress. Pp. 10–60 in: *Low-grade Metamorphism* (M. Frey and D. Robinson, editors). Blackwell Sciences, Oxford, UK.

Mingram, B., Hoth, P., Lüders, V. and Halrov, D. (2005) The significance of fixed ammonium in Palaeozoic sediments for the generation of nitrogen-rich natural gases in the North German Basin. *International Journal of Earth Sciences*, **94**, 1010–1022.

Moore, J.C. (1989) Tectonics and hydrogeology of accretionary prisms: role of the décollement zone. *Journal of Structural Geology*, **11**, 95–106.

Muchez, Ph., Slobodnik, M., Viaene, W. and Keppens, E. (1994) Mississippi Valley-type Pb-Zn mineralization in eastern Belgium: Indications for gravity-driven flow. *Geology*, **22**, 1011–1014.

Nierhoff, R. (1994) Metamorphose-Entwicklung im Linksrheinischen Schiefergebirge: Metamorphosegrad und –verteilung sowie Metamorphosealter nach K-Ar-Datierungen. *Aachener Geowissenschaftliche Beiträge*, **3**, 1–159.

Nieto, F. (2002) Characterization of coexisting NH_4- and K-micas in very low-grade metapelites. *American Mineralogist*, **87**, 205–216.

Oliver, J. (1986) Fluids expelled tectonically from orogenic belts: Their role in hydrocarbon migration and other geological phenomena. *Geology*, **14**, 99–102.

Oncken, O. (1989) Geometrie, Deformationsmechanismen und Paläospannungsgeschichte großer Bewegungszonen in der höheren Kruste (Rheinisches Schiefergebirge). *Geotektonische Forschungen*, **73**, 1–215.

Oncken, O., von Winterfeld, C. and Dittmar, U. (1999) Accretion of a passive margin: The late Paleozoic Rhenohercynian fold and thrust belt (Middle European Variscides). *Tectonics*, **18**, 75–91.

Österreich, B., Ribbert, K.H. and Wrede, V. (2005) Erste Ergebnisse zur biostratigrafischen und tektonischen Einordnung der Bohrung RWTH-1. Unpublished report, GD-NRW, 2005.

Pironon, J., Pelletier, M., de Donato, P. and Mosser-Ruck, R. (2003) Characterization of smectite and illite by FTIR spectroscopy of interlayer NH_4^+ cations. *Clay Minerals*, **38**, 201–211.

Pollastro, R.M. (1993) Considerations of the illite-smectite geothermometer in hydrocarbon-bearing rocks of Miocene to Mississippian age. *Clays and Clay Minerals*, **41**, 119–133.

Rao, S. and Houska, C.R. (1986) X-ray diffraction profiles described by refined analytical functions. *Acta Crystallographica*, **A42**, 14–19.

Redecke, P. (1992) Zur Geochemie und Genese variszischer und postvariszischer Buntmetallmineralisation in der Nordeifel und der Niederrheinischen Bucht. *Mitteilungen zur Mineralogie und Lagerstättenkunde*, **41**, Aachen, 152 pp.

Reynolds, R.C. Jr., Distefano, M.P. and Lahann, R.W. (1992) Randomly interstratified serpentine/chlorite: Its detection and quantification by powder X-ray diffraction methods. *Clays and Clay Minerals*, **40**, 262–267.

Robinson, D. and Merriman, R.J. (1999) Low-temperature metamorphism: an overview. Pp. 1–9 in: *Low-grade Metamorphism* (M. Frey and D. Robinson, editors). Blackwell Sciences, Oxford.

Rottke, W. and Stroink, L. (1999) Die Genese devonischer Vorlandsedimente am NW-Rand des Rheinischen Massivs – Zement- und Porenraumentwicklung. *Zeitschrift der deutschen Gesellschaft für Geowissenschaften*, **150**, 471–491.

Scherrer, P. (1918) Bestimmung der Größe und der inneren Struktur von Kolloidteilchen mittels Röntgenstrahlen. *Göttinger Nachrichten*, **2**, 98–100.

Schneider, J., Haack, U., Hein, U.F. and Germann, A. (1999) Direct Rb/Sr dating of sandstone-hosted sphalerites from stratabound Pb-Zn deposits in the northern Eifel, NW Rhenish Massif, Germany. Pp. 1287–1290 in: *Mineral Deposits: Processes to Processing. Proceedings of the 5th Biennial. SGA Meeting and the 10th Quadrennial IAGOD Symposium* (C.J. Stanley, editor). London, 22–25 August, 1999.

Smith, R.E. and Wiltschko, D.V. (1996) Generation and maintenance of abnormal fluid pressures beneath a ramping thrust sheet: isotropic permeability experiments. *Journal of Structural Geology*, **18**, 951–970.

Środoń, J., Elsass, F., McHardy, W.J. and Morgan, D.J. (1992) Chemistry of illite-smectite inferred from TEM measurements of fundamental particles. *Clay Minerals*, **27**, 137–158.

Środoń, J., Morgan, D.J., Eslinger, E.V., Eberl, D.D. and Karlinger, M.R. (1986) Chemistry of illite/smectite and end member illite. *Clays and Clay Minerals*, **34**, 368–378.

Stanjek, H. and Häusler, W. (2000) Quantifizierung silikatischer Tonminerale im Textur- und Pulverpräparat mit MacClayFit. *Berichte der Deutschen Ton- und Tonmineralgruppe e.V.*, **7**, 256–265.

Steingrobe, B. (1990) Fazieseinheiten aus dem Aachen-Erkelenzer Oberkarbonvorkommen unter besonderer Berücksichtigung des Inde-Synklinoriums. Dissertation RWTH-Aachen, Germany, 325 pp.

Šucha, V., Elsass, F., Eberl, D.D., Kuchta, L., Madejová, J., Gates, W.P. and Komadel, P. (1998) Hydrothermal synthesis of ammonium illite. *American Mineralogist*, **83**, 58–67.

Teichmüller, M. and Teichmüller, R. (1979) Ein Inkohlungsprofil entlang der linksrheinischen Geotraverse von Schleiden nach Aachen und die Inkohlung in der Nord-Süd-Zone der Eifel. *Forschritte Geologie Rheinland und Westfalen*, **27**, 323–355.

Thompson, P., Cox, D.E. and Hastings, J.B. (1987) Rietveld refinement of Debye-Scherrer synchroton X-ray data of Al_2O_3. *Journal of Applied Crystallography*, **20**, 79–83.

Tschernoster, R., Glasmacher, U., Spaeth, G. and Clauer, N. (1995) K-Ar- Datierungen zur Abkühlungsgeschichte ausgewählter Magmatite und Metapelite aus dem Stavelot Venn Massiv. Pp. 1–20 in: *KW-relevante Eigenschaften potentieller Mutter- und Speichergesteine am Nordrand des Linksrheinischen Schiefergebirges* (R. Walter, U. Glasmacher and M. Wolf, editors). RWTH-Aachen, BMBF Forschungsprojekt 032 6804 A 5, Teil 4.

Velde, B. and Lanson, B. (1993) Comparison of I/S transformation and maturity of organic matter at elevated temperatures. *Clays and Clay Minerals*, **41**, 178–183.

Vogtmann-Becker, J. (1990) Mobilisation und Austausch von Elementen durch Regionalmetamorphose in kambro-ordovizischen Sedimentgesteinen des Stavelot-Venn-Massivs. *Mitteilungen zur Mineralogie und Lagerstättenlehre*, **34**, 1–179.

Von Winterfeld, C.-H. (1994) Variszische Deckentektonik und devonische Beckengeometrie der Nordeifel – Ein quantitatives Modell. *Aachener Geowissenschaftliche Beiträge*, **2**, 319 pp.

Wang, H., Frey, M. and Stern, W.B. (1996) Diagenesis and metamorphism of clay minerals in the Helvetic Alps of eastern Switzerland. *Clays and Clay Minerals*, **44**, 96–112.

Warr, L.N. (1996) Standardized clay mineral crystallinity data from the very low-grade metamorphic facies rocks of southern New Zealand. *European Journal of Mineralogy*, **8**, 115–127.

Warr, L.N. and Rice, A.H.N. (1994) Interlaboratory standardization and calibration of clay mineral crystallinity and crystallite size data. *Journal of Metamorphic Geology*, **12**, 141–152.

Warr, L.N. and Nieto, F. (1998) Crystallite thickness and defect density of phyllosilicates in low-temperature metamorphic pelites: A TEM and XRD study of clay-mineral crystallinity-index standards. *The Canadian Mineralogist*, **36**, 1453–1474.

Weaver, C.E. (1960) Possible uses of clay minerals in search for oil. *Bulletin of the American Association of Petroleum Geologists*, **44**, 1505–1518.

Williams, L.B., Ferrell, R.E., Chinn, E.W. and Sassen, R. (1989) Fixed-ammonium in clays associated with crude oils. *Applied Geochemistry*, **4**, 605–616.

Wilson, P.N., Parry, W.T. and Nash, W.P. (1992) Characterization of hydrothermal tobelitic veins from black shale, Oquirrh Mountains, Utah. *Clays and Clay Minerals*, **40**, 405–420.

Yau, Y.C., Peacor, D.R., Bearne, R.e., Essene, E.J. and McDowell, S.D. (1988) Microstructures, formation mechanisms, and depth-zoning of phyllosilicates in geothermally altered shales, Salton Sea, California. *Clays and Clay Minerals*, **36**, 1–10.

Zhang, Y., Muchez, Ph. and Hein, U.F. (1997) Chlorite geothermometry and the temperature conditions at the Variscan thrust front in eastern Belgium. *Geologie en Mijnbouw*, **76**, 267–270.

(*Received 25 July 2006; revised 11 December 2006; Ms. 1194; A.E. Ray E. Ferrell Jr.*)